International Journal of Geo-Information

MDPI

Article

SSIEGNOS: A New Asian Single Site Tropospheric Correction Model

Liangke Huang [1,2], Shaofeng Xie [1,2,*], Lilong Liu [1,2,3,*], Junyu Li [1,2], Jun Chen [1,2] and Chuanli Kang [1,2]

1 College of Geomatics and Geoinformation, Guilin University of Technology, Guilin 541004, China; lkhuang@glut.edu.cn (L.H.); yl_lijunyu@163.com (J.L.); Snake90@126.com (J.C.); kcl79@126.com (C.K.)
2 Guangxi Key Laboratory of Spatial Information and Geomatics, Guilin 541004, China
3 College of Resources and Environment, Qinzhou University, Qinzhou 535011, China
* Correspondence: xieshaofeng@glut.edu.cn (S.X.); hn_liulilong@163.com (L.L.)

Academic Editors: Zhao-Liang Li, Jose A. Sobrino, Chao Ren and Wolfgang Kainz
Received: 13 August 2016; Accepted: 9 January 2017; Published: 17 January 2017

Abstract: This paper proposes a new Asian single site tropospheric correction model called the Single Site Improved European Geostationary Navigation Overlay Service model (SSIEGNOS) by refining the European Geostationary Navigation Overlay Service (EGNOS) model at a single site. The performance of the SSIEGNOS model is analyzed. The results show that (1) the bias and root mean square (RMS) error of zenith tropospheric delay (ZTD) calculated from the EGNOS model are 0.12 cm and 5.87 cm, respectively; whereas those of the SSIEGNOS model are 0 cm and 2.52 cm, respectively. (2) The bias and RMS error show seasonal variation in the EGNOS model; however, little seasonal variation is observed in the SSIEGNOS model. (3) The RMS error decreases with increasing altitude or latitude in the two models; however, no such relationships were found in the bias. In addition, the annual predicted bias and RMS error in Asia are −0.08 cm and 3.14 cm for the SSIEGNOS model, respectively; however, the EGNOS and UNB3m (University of New Brunswick) models show comparable predicted results. Relative to the EGNOS model, the annual predicted bias and RMS error decreased by 55% and 48%, respectively, for the SSIEGNOS model.

Keywords: Asia; EGNOS model; SSIEGNOS model; zenith tropospheric delay; accuracy analysis

1. Introduction

Tropospheric delay is the dominant error source in Global Navigation Satellite System (GNSS) technologies, which can be as high as approximately 2 m in the zenith direction for the propagating radio signal. This error becomes higher as the propagating direction deviates from the zenith towards the horizon direction and can reach approximately 20 m at the horizon direction [1]. Therefore, tropospheric delay must be effectively corrected when used for real-time GNSS navigation and positioning, especially when applied in GNSS real-time precise point positioning techniques [2,3]. In addition, Tropospheric delay is an important parameter in tropospheric tomography and GNSS meteorology [4–7]. Empirical tropospheric correction models, such as the Hopfield model and Saastamoinen model, can be used to calculate the tropospheric delay at arbitrary sites based on the provided meteorological data. However, both models require real-time meteorological parameters for the calculations because using standard meteorological parameters results in poor accuracy. Thus, it is obvious that they cannot satisfy real-time tropospheric delay correction for space geodetic techniques.

In recent years, an effective method to calculate the zenith tropospheric delay (ZTD) has been generated using the National Center for Environmental Prediction (NCEP) reanalysis data or the European Center for Medium-range Weather Forecasts (ECMWF) reanalysis data [8–11]. A number of studies have been conducted to assess the ZTD derived from reanalysis datasets. For example,

Chen et al. [12,13] assessed the feasibility and accuracy of the ECMWF/NCEP data for tropospheric delay correction in China and Asia. The research results demonstrated that the ECMWF reanalysis datasets exhibited a higher accuracy than the NCEP reanalysis datasets when used to calculate the ZTD. Similarly, several tropospheric models have been developed using ECMWF or NCEP datasets in North America and the European Union. For instance, Collins et al. [14] introduced the UNB3 (University of New Brunswick) model, which considers the major changes in water vapor profiles with latitude; it has been widely applied in the Wide Area Augmentation System (WAAS) in the United States. In North America, the bias is as high as 20 cm for the ZTD derived from UNB3 model, with a mean bias of approximately 2 cm. Krueger et al. [15] established a TropGrid model with the NCEP datasets, which takes annual and diurnal variations for variables such as temperature into account, resulting in a root mean square (RMS) error of the ZTD of 3.8 cm. Schuler [16] developed the TropGrid2 version by improving the former TropGrid model; however, the new version is only marginally (1 mm) more accurate than the old version on a global scale. Lagler et al. [17] developed a new model, GPT2, to improve the Global Pressure Temperature (GPT) [18]. GPT2 is based on a more precise ECMWF ERA-Interim, and takes semi-annual variation into consideration, which can provide pressure, temperature, and other key tropospheric parameters. Boehm et al. [19] proposed an improved model, GPT2w, which adds the water vapor lapse rate and weighted mean temperature (Tm) and improves horizontal resolution compared to GPT2. In addition, Li et al. [1] built a global ZTD model (named the IGGtrop model) using NCEP reanalysis data, which shows a higher accuracy than the UNB3 and UNB3m models. Yao et al. [20,21] proposed several global ZTD models based on the ECMWF ERA-Interim. New models present a higher accuracy in global terms.

Similar to the UNB3 model, the European Union recommended the European Geostationary Navigation Overlay Service (EGNOS) model, which was also derived from ECMWF datasets [22]. The EGNOS model has been largely applied in the United States and the European Union for the WAAS, and its performance has been investigated in both North America and Europe, with maximum RMS errors ranging from 13.2 to 17.8 cm [23]. These empirical models, such as EGNOS and UNB series models, present higher mean correction global accuracy.

Extensive investigations have been conducted to evaluate the ZTD derived from multi-techniques. For example, Bock et al. [24] and Teke et al. [25] indicated that the ZTDs derived from GPS and Doppler Orbitography and Radio-positioning Integrated by Satellite (DORIS) exhibited a higher correlation coefficient. Similar studies published by Wei et al. [26] and Ning et al. [27] showed that the ZTDs from GPS and Very Long Baseline Interferometry (VLBI) display strong agreement, with a correlation coefficient higher than 0.87. In addition, space geodetic techniques, such as GNSS, VLBI, and DORIS, are affected by the same tropospheric delays when considering the height differences at co-located sites [28]. Recently, the multi-techniques, such as GNSS, VLBI, and DORIS, have been largely applied in real time precise orbit determination of satellites or aircrafts [29,30]. For example, the successful running of the China Chang'E series aircrafts is mainly dependent on the precise orbits [31]. Because the precise orbit is related to the precise tropospheric correction in data processing of space techniques, it is therefore extremely important to improve the precision of empirical models, such as the EGNOS and UNB series models, for real-time tropospheric correction at each of the GNSS, VLBI, and DORIS stations at regional scales. Nowadays, there are about 25 VLBI sites and 13 DORIS sites were established in Asia (http://ggosatm.hg.tuwien.ac.at/products.html); the number of stations at co-located international GNSS service (IGS) sites is increasing. In addition, the precise zenith tropospheric correction in data processing of VLBI, or a combination of VLBI and GNSS, can lead to an improvement in station coordinates repeatability [32–34] and especially to an improvement in station height [35]. The main purpose of this paper is to refine the EGNOS model at a single site using the IGS ZTD data of Asia and to establish a Single Site Improved European Geostationary Navigation Overlay Service model (named the SSIEGNOS model) that can function without any meteorological data.

2. Determination of the SSIEGNOS Model

2.1. Data Sources

The EGNOS tropospheric correction model was constructed by the European Geostationary Navigation Overlay Service. Without any real measured meteorological parameters to calculate the ZTD, it only relies on the pressure, temperature, water vapor pressure, temperature gradient, and water vapor pressure gradient. The functions in the EGNOS model are described in Penna et al. [23].

In this paper, we utilize the ZTD data from 2008–2012, observed from 46 IGS sites distributed in Asia (ftp://cddis.gsfc.nasa.gov/pub/gps/products/), with a temporal resolution of 5 min and an approximately 4 mm calculating accuracy of the ZTD [36,37]. The study area approximately covers the area from 10° N~63° N in latitude and 30° E~160 °E in longitude. The locations of the IGS sites are shown in Figure 1.

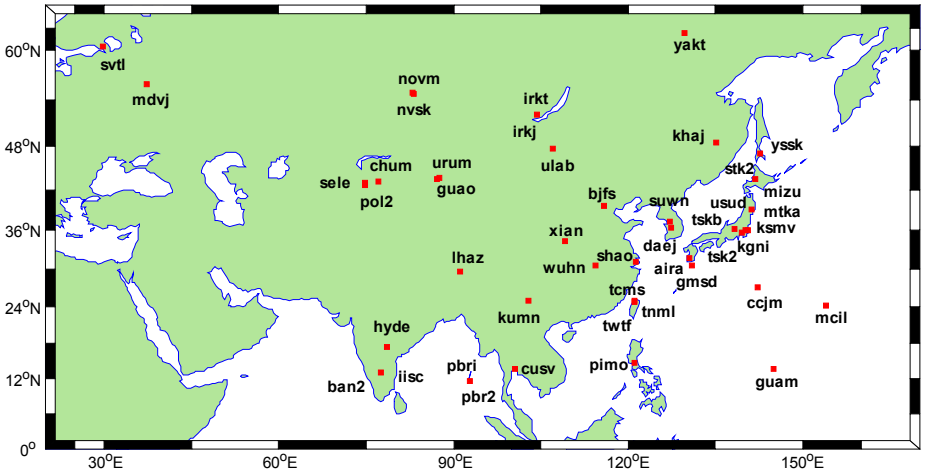

Figure 1. Distribution of the IGS sites in Asia. The abscissa represents longitude, and the ordinate represents latitude.

2.2. Establishment of the SSIEGNOS Model

In this study, the ZTD data from 2008–2010 observed from 46 IGS sites distributed in Asia are regarded as the reference values. The annual mean values and seasonal variation values of the five meteorological parameters of the EGNOS model can be calculated, as described in Penna et al. [23]. Three years of daily biases of the ZTD, derived from the EGNOS model, were obtained by comparison with the reference ZTD values. An obvious phenomenon is detected from the spectral analysis for the ZTD daily bias using fast Fourier transformation; the variation of daily bias exhibits an annual cycle at the sites located lower than 30 degrees latitude in Asia. However, an annual cycle and a semi-annual cycle are shown at the sites higher than 30 degrees latitude in Asia. The results of the spectral analysis among all 6 of the IGS sites in Asia are shown in Figure 2. Figure 2 shows that the daily bias can be approximately expressed by the cosine function, according to the following formula:

$$Bias(\varphi_i, \lambda_i, t) = \begin{cases} Bias_{mean}(\varphi_i, \lambda_i) + Amp1(\varphi_i, \lambda_i) \cdot \cos\left(\frac{2\pi}{365.25}(t - d1(\varphi_i, \lambda_i))\right) + \psi(t), \ \varphi_i < 30^\circ N \\ Bias_{mean}(\varphi_i, \lambda_i) + Amp1(\varphi_i, \lambda_i) \cdot \cos\left(\frac{2\pi}{365.25}(t - d1(\varphi_i, \lambda_i))\right) \\ + Amp2(\varphi_i, \lambda_i) \cdot cos\left(\frac{4\pi}{365.25}(t - d2(\varphi_i, \lambda_i))\right) + \xi(t), \ \varphi_i \geq 30^\circ N \end{cases} \quad (1)$$

where t and $Bias(\varphi_i, \lambda_i, t)$ are the day of year and daily bias (which are treated as known parameters); $Bias_{mean}(\varphi_i, \lambda_i)$ is the annual mean bias; $Amp1(\varphi_i, \lambda_i)$ and $Amp2(\varphi_i, \lambda_i)$ are the amplitudes of the annual and semi-annual component, respectively; $d1(\varphi_i, \lambda_i)$ and $d2(\varphi_i, \lambda_i)$ are the phases of the annual

and semi-annual components, respectively; $\psi(t)$ and $\xi(t)$ are the residuals; and φ is the site's latitude. The unknown parameters ($Bias_{mean}(\varphi_i, \lambda_i)$, $Amp1(\varphi_i, \lambda_i)$, $Amp2(\varphi_i, \lambda_i)$, $d1(\varphi_i, \lambda_i)$, and $d2(\varphi_i, \lambda_i)$) in Equation (1) are estimated based on the nonlinear least squares method using three years of daily bias data at each IGS site.

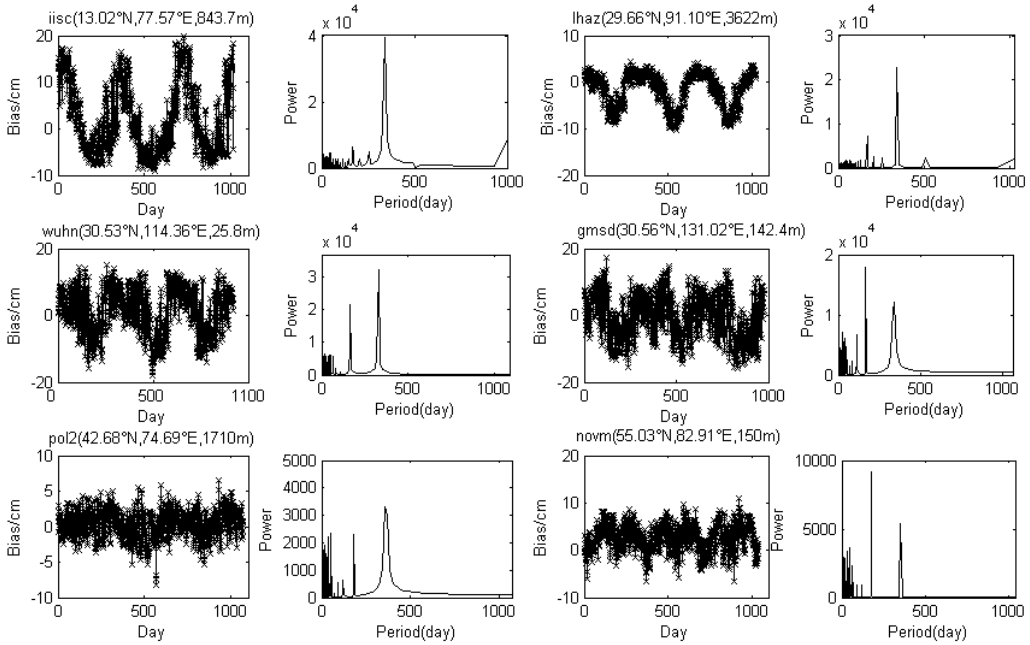

Figure 2. Variation of the daily bias and spectral analysis based on Fourier transformation at IISC, LHAZ, WUHN, GMSD, POL2 and NOVM sites in 2008–2010. The latitude, longitude, and altitude of each site are listed in the brackets.

As analyzed above, the formula of the SSIEGNOS model can be expressed as follows:

$$ZTD_{SSIEGNOS} = ZTD_{EGNOS} - Bias(\varphi_i, \lambda_i, t) \quad (2)$$

where ZTD_{EGNOS} denotes the ZTD derived from the EGNOS model; $Bias(\varphi_i, \lambda_i, \mathrm{t})$ is the ZTD correction value of the EGNOS model, which can be calculated by Equation (1); and $ZTD_{SSIEGNOS}$ is the ZTD derived from the SSIEGNOS model.

3. SSIEGNOS Model Validation

As analyzed in Section 2, the ZTD biases between IGS, ZTD, and ZTD derived from EGNOS present obvious annual cycles and a semi-annual cycles. So, the ZTD biases can be modeled using the cosine or sinusoidal function, and the SSIEGNOS model can also be developed. In this section, to validate the SSIEGNOS model, the ZTD data from 2008–2010, obtained from 46 IGS sites distributed in Asia, are treated as the reference values. The results are compared with those of the EGNOS model. The accuracy and stability of the newly proposed SSIEGNOS and another two models are assessed using two indices: bias, the error between the model values and the reference values; and RMS, the accuracy and stability of the model. The bias and RMS error of the temporal and spatial distribution characteristics are analyzed. The formulas for bias and RMS as follows:

$$bias = \frac{1}{N}\sum_{i=1}^{N}\left(ZTD_m^i - ZTD_{IGS}^i\right) \quad (3)$$

$$RMS = \sqrt{\frac{1}{N}\sum_{i=1}^{N}\left(ZTD_m^i - ZTD_{IGS}^i\right)^2} \quad (4)$$

where ZTD_m^i is the value calculated by the EGNOS and SSIEGNOS models, ZTD_{IGS}^i is the reference value derived from the IGS tropospheric products, and N is the number of ZTD calculations.

3.1. The Temporal Variation of the Bias and RMS Error

3.1.1. Variation of the Daily Bias and RMS Error

To analyze the variation of the daily bias and RMS error of the SSIEGNOS and EGNOS models, the bias and RMS error at each site were analyzed for each day. Figure 3 shows the variation of the daily bias and RMS error of the SSIEGNOS and EGNOS models at sites IRKJ (Northern Asian), CHUM (Western Asian), TSK2 (Eastern Asian), and CUSV (Southern Asian), respectively. The bias and RMS error at other sites presented similar characteristics.

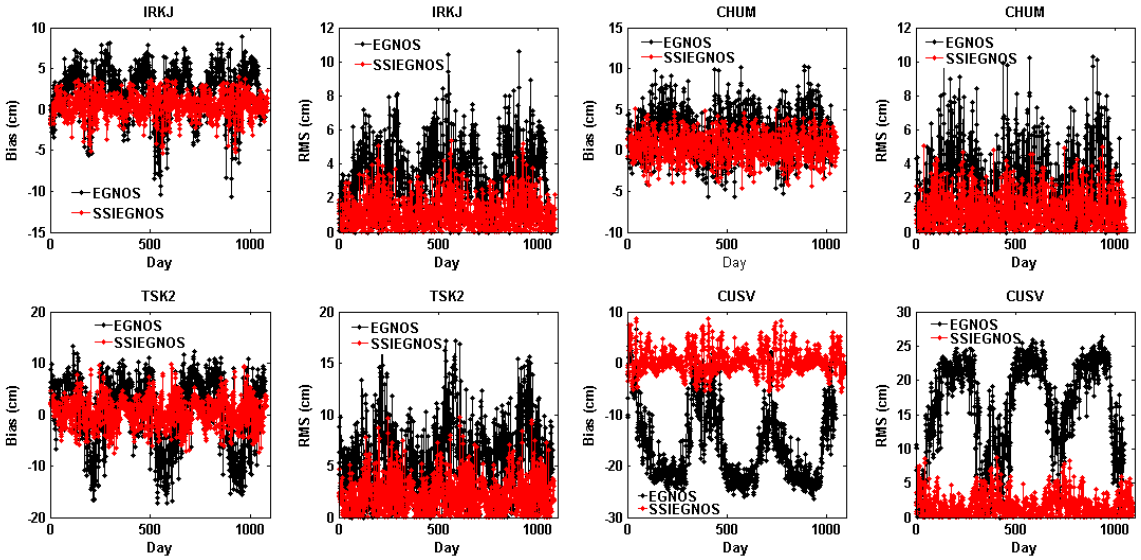

Figure 3. Variation of the daily bias and RMS in 2008–2010 at sites IRKJ, CHUM, TSK2, and CUSV for the EGNOS and SSIEGNOS models. The black line represents EGNOS model and the red line represents SSIEGNOS model.

Figure 3 shows an obvious cyclic behavior in the daily bias and RMS error in the EGNOS model, reaching maximum values in summer. We also find that the daily bias and RMS error at the CHUM site (located in western Asia) has lower variation relative to the other sites. Moreover, the TSK2 site is located on the border of the ocean and the land and thus presents larger amplitudes of bias and RMS error in eastern Asia, due to the effect of the maritime climate and the dramatic changes in atmospheric water vapor. Greater variation is also observed in summer at the CUSV site, which is adjacent to the low-latitude area of southern Asia and is mainly affected by tropical and maritime climate regimes. The SSIEGNOS model shows stable and small variation in terms of the bias and RMS error; smaller fluctuations are observed in the summer over eastern and southern Asia. Overall, these results show a remarkable correction result from the EGNOS model.

3.1.2. Variation of the Monthly Bias and RMS Error

In order to analyze the monthly variation of the bias and RMS for the SSIEGNOS and EGNOS models, three years of bias and RMS at 46 sites, from 2008 to 2010, are used for monthly and seasonal statistics. The statistical results are shown in Figure 4 and Table 1.

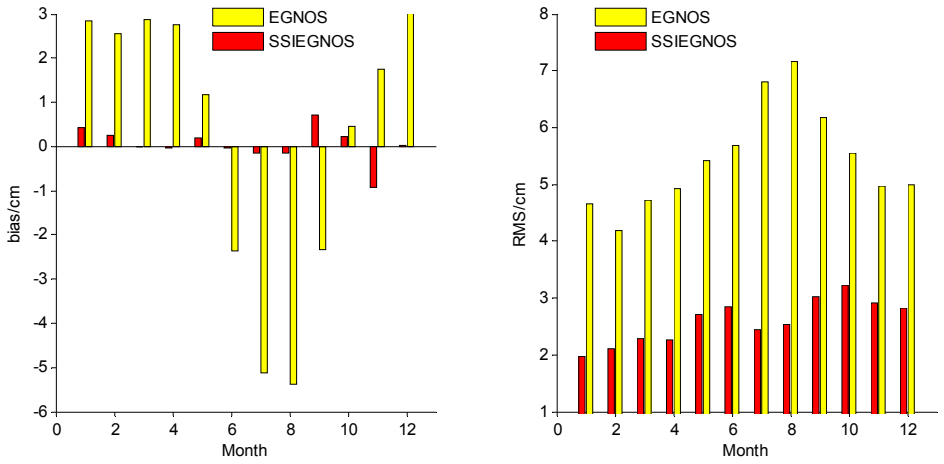

Figure 4. Variation of the monthly bias and RMS error in 2008–2010 over Asia. Yellow bars and red bars indicate the bias and RMS error of the EGNOS model and SSIEGNOS model, respectively.

Table 1. Seasonal variation of the bias and RMS error of the EGNOS and SSIEGNOS models in 2008–2010 over Asia (Unit: cm).

Season	EGNOS		SSIEGNOS	
	Bias	**RMS**	**Bias**	**RMS**
Spring	2.27	5.02	0.05	2.42
Summer	−4.29	6.55	0.10	2.60
Autumn	−0.05	5.56	0.01	3.06
Winter	2.86	4.61	0.23	2.30

Figure 4 shows obvious seasonal variation of the bias and RMS error for the EGNOS model. The bias and RMS error have larger values in summer and relatively lower variation in other seasons. A negative maximum bias occurs in August due to the effect of the changeable atmospheric water vapor. The SSIEGNOS model also shows that the monthly bias and RMS error are irregular in all months, with lower overall variation. Hence, the SSIEGNOS model can achieve an outstanding correction result compared with the EGNOS model.

Table 1 shows that, in the EGNOS model, the maximum bias occurs in summer and the minimum bias occurs in autumn. The RMS error also reaches a maximum in summer and a minimum in winter. In the SSIEGNOS model, the maximum bias occurs in winter and the minimum occurs in autumn, whereas the RMS error reaches a maximum in autumn and a minimum in winter. In addition, it presents a stable variation in all seasons.

3.1.3. Variation of the Annual Bias and RMS Error

Three years of bias and RMS error from 2008 to 2010 at 46 sites are used to analyze the annual statistics of the EGNOS and SSIEGNOS models. The distributions of the annual bias and RMS error of the EGNOS and SSIEGNOS models are presented in Figure 5. Figure 5 suggests that the annual bias and RMS error have larger variation in eastern and southern Asia and relatively smaller variation in western and northern Asia in the EGNOS model. In the SSIEGNOS model, the bias and RMS error display lower variation over Asia, especially in the western and high-latitude areas of northern Asia, where the RMS error is lower than 2 cm, which suggests that the SSIEGNOS model can be applied to study the high precision zenith tropospheric delay in these areas. Compared with ZTD derived from the IGS center, the precision of ZTD calculated from the SSIEGNOS model is better than that of the EGNOS model over Asia. In the SSIEGNOS model, the bias and RMS error are 0.00 cm and 2.52 cm, respectively, whereas those of the EGNOS model are 0.12 cm and 5.87 cm, respectively. Therefore,

relative to the EGNOS model, the absolute bias and RMS error of the SSIEGNOS model are decreased by 99% and 62% at sites lower than 30 degrees latitude, respectively, and decreased by 99% and 54% at sites higher than 30 degrees latitude, respectively, with an overall decrease of 99% and 57% in Asia, respectively. These results indicate that the SSIEGNOS model has a significantly superior correction ability relative to the EGNOS model in Asia, especially in the low-latitude areas. In addition, we also find that the annual RMS error of the SSIEGNOS and EGNOS models decreases with increasing latitude. This finding will be further studied in the following section.

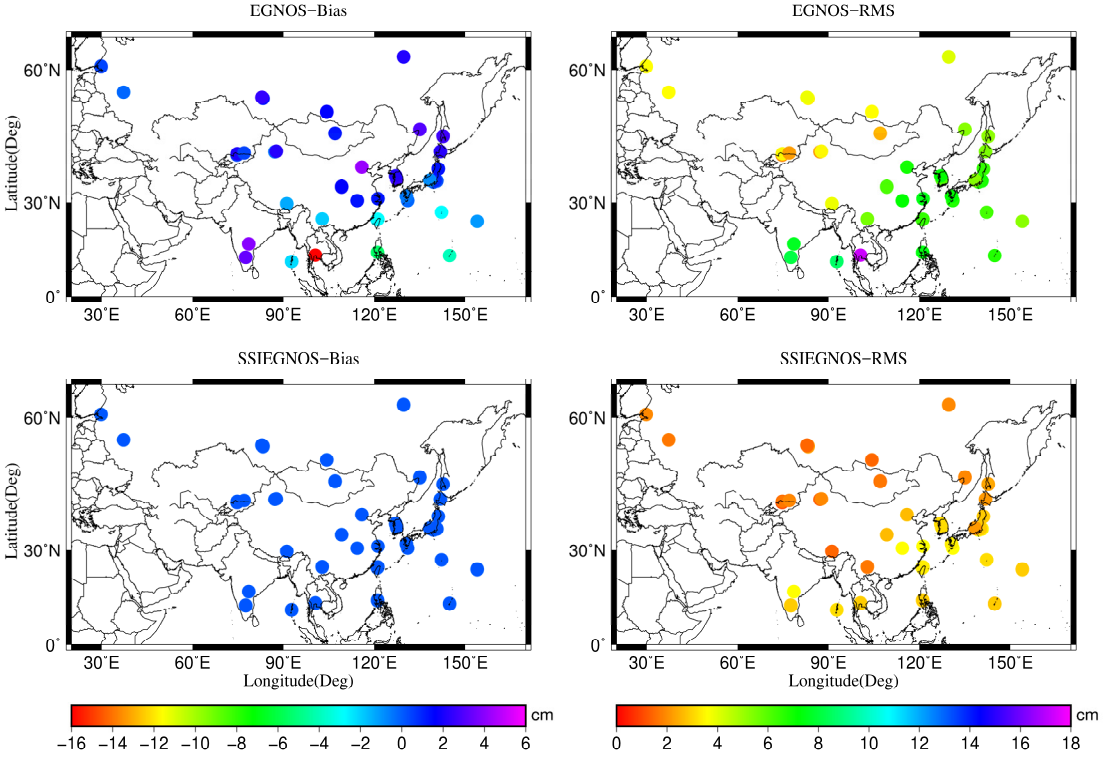

Figure 5. Distribution of annual bias and RMS error of the EGNOS and SSIEGNOS models from 2008–2010 over Asia. The color denotes the magnitude of the annual bias and RMS error.

3.2. Spatial Characteristics of Annual Bias and RMS Error

3.2.1. Relations between the Altitude and the Annual Bias and RMS Error

The ZTD variation is complex due to the strong correlation between ZTD and altitude over the fluctuating terrain of Asia. In order to investigate the relation between the annual bias and RMS error with altitude, 46 IGS sites were sorted into five categories based on altitude; less than 500 m, 500~1000 m, 1000~1500 m, 1500~2000 m, and above 2000 m. The variation of the annual bias and RMS error in each altitude range is shown in Figure 6.

Figure 6 shows that the annual bias is not obvious with increasing altitude in the SSIEGNOS and EGNOS models; however, the annual bias exhibits a slight correlation with altitude. In general, the annual RMS error decreases with increasing altitude in both the SSIEGNOS and EGNOS models, but, in the altitude range of 1000~1500 m, this effect is lower in the EGNOS model.

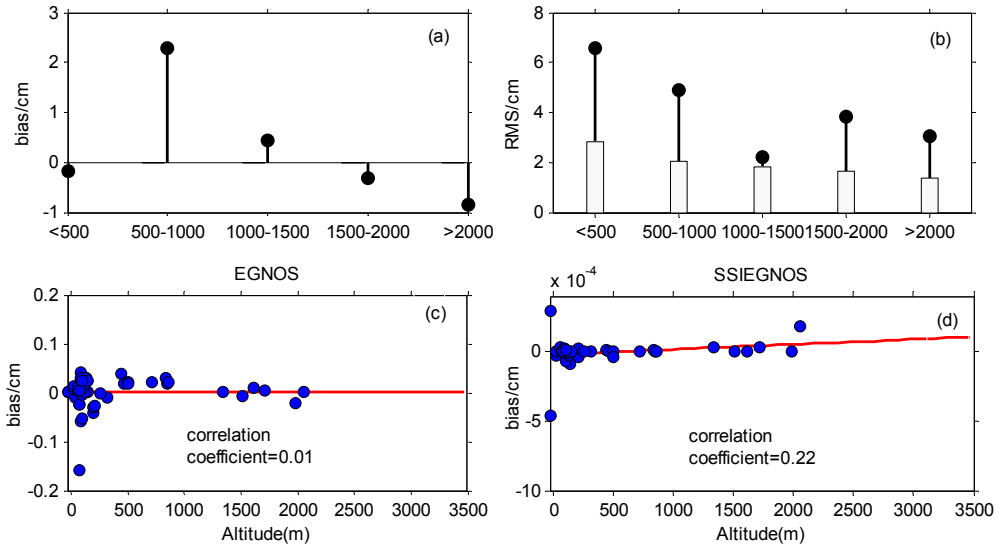

Figure 6. (**a**,**b**) show the annual bias and RMS error in each altitude range, respectively; (**c**,**d**) denote the correlations between altitude and bias and RMS error, respectively. Black stems and white bars represent the mean bias and RMS error of the EGNOS and SSIEGNOS models, respectively.

3.2.2. Relations between Latitude and the Annual Bias and RMS Error

The variation of ZTD is complicated due to the complex topography and climate over the wide distribution of land and water in Asia. The relations between latitude and the annual bias and RMS error in the SSIEGNOS and EGNOS models are analyzed.

To visualize the variation of the annual bias and RMS error, 46 IGS sites were sorted in terms of latitude in 10-degree intervals, i.e. 10°~20°, 20°~30°, 30°~40°, 40°~50°, and above 50°. The results are shown in Figure 7.

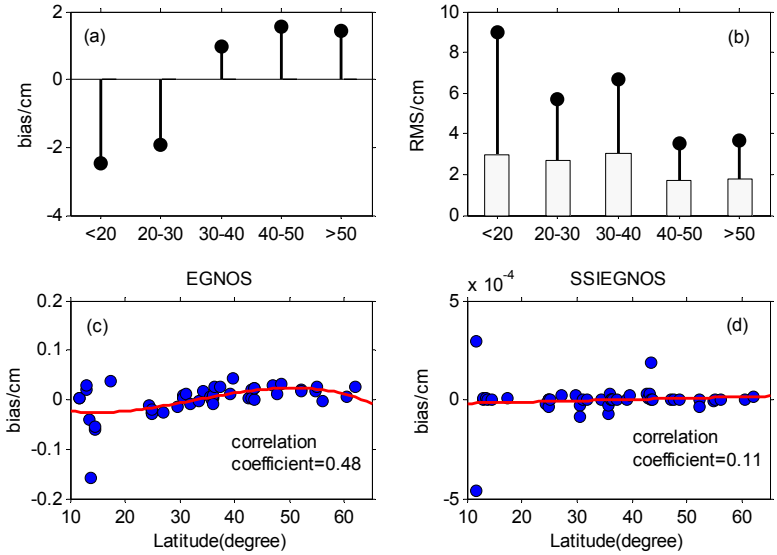

Figure 7. (**a**,**b**) show the annual bias and RMS error in each latitude range; (**c**,**d**) show the correlations between bias and latitude, respectively. Black stems and white bars denote the mean bias and RMS error of the EGNOS and SSIEGNOS models, respectively.

Figure 7 indicates that the annual RMS error decreases with increasing latitude in both the SSIEGNOS and EGNOS models. However, Figure 7c,d show apparently that the annual bias has a small correlation with latitude in both models.

3.2.3. Relations between Longitude and the Annual Bias and RMS Error

To study the relations between longitude and the annual bias and RMS error for the SSIEGNOS and EGNOS models, 46 IGS sites were sorted by longitude using 10-degree intervals: less than 80°, 80°~90°, 90°~100°, 100°~110°, 110°~120°, 120°~130°, 130°~140°, and above 140°. In addition, the correlations between the annual bias and longitude are also analyzed. The results are shown in Figure 8.

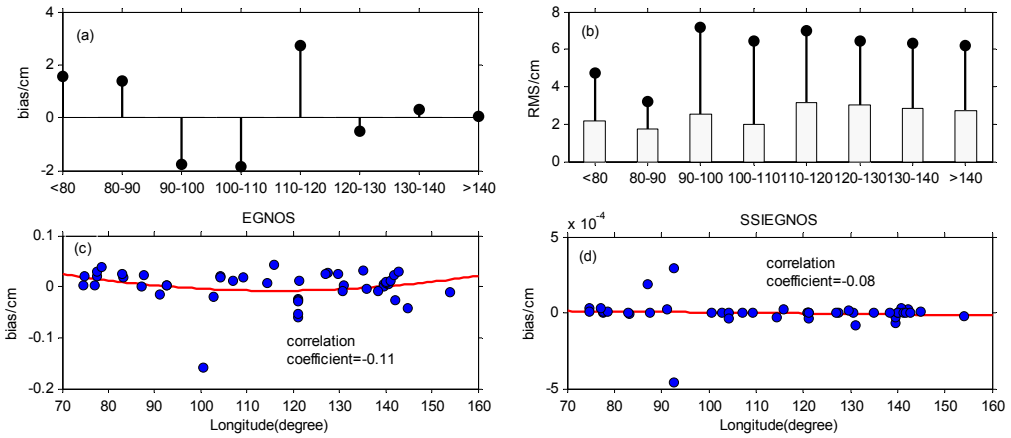

Figure 8. (**a**,**b**) show the annual bias and RMS error in each longitude range; whereas (**c**,**d**) show the mean correlations between bias and longitude. Black stems and white bars represent the mean bias and RMS error of the EGNOS and SSIEGNOS models, respectively.

Figure 8 shows the irregular relationships between longitude and the annual bias and RMS error of the SSIEGNOS and EGNOS models. The annual bias presents a small correlation with longitude according to the correlation coefficient.

3.3. Assessment of Predicted ZTD Derived from the SSIEGNOS Model

3.3.1. The Performance of the SSIEGNOS Model for Predicting ZTD

To validate the precision of the predicted ZTD using the SSIEGNOS model, one year of ZTD data from 2011, with higher accuracy, were derived from 46 IGS sites distributed in Asia and are regarded as reference values; the predicted precision of SSIEGNOS model is compared with the EGNOS and UNB3m models. The predicted ZTDs were derived from the SSIEGNOS, EGNOS, and UNB3m models; the details of the functions in the UNB3m model are described in Leandro et al. [38]. The results are compared with the ZTD data provided by the IGS center. The distribution of the predicted bias and RMS error of the EGNOS, UNB3m, and SSIEGNOS models over Asia are shown in Figure 9, and the statistical results are shown in Table 2 and Figure 10.

Table 2 shows the value range and annual mean values of the bias and RMS error of the predicted ZTD calculated from the EGNOS, UNB3m, and SSIEGNOS models in Asia. As observed in Table 2, the ZTD can be predicted at the centimeter level by the SSIEGNOS model. The annual mean bias and RMS error of the SSIEGNOS model are −0.1 cm and 3.1 cm, respectively, which are lower than those of the EGNOS and UNB3m models. Figure 9 demonstrates that the predicted bias of both the EGNOS model and UNB3m model are lower in central Asia and greater in eastern Asia and at lower latitudes, whereas the predicted bias of the SSIEGNOS is low in all of Asia. The EGNOS model and the UNB3m model show comparable results, which have a greater predicted RMS error in Asia; an RMS of approximately 4 cm occurs in the high-latitude area of northwestern Asia. The SSIEGNOS model has

a predicted RMS better than 3 cm at sites higher than 30 degrees latitude. Slightly poorer results are observed in the low latitudes of southern and eastern Asian. However, significant correction results can still be achieved in these regions, with an RMS error lower than 5 cm. Relative to the EGNOS model, the annual absolute bias and RMS error of the predicted ZTD of the SSIEGNOS model are decreased by 95% and 54% at sites lower than 30 degrees latitude, respectively, and decreased by 94% and 45% at sites higher than 30 degree latitude, respectively. Hence, the annual absolute bias and RMS of the predicted ZTD are decreased by 55% and 48% in all of Asia, respectively. This indicates that higher predicted precision can be obtained at latitudes lower than 30 degrees in the SSIEGNOS model.

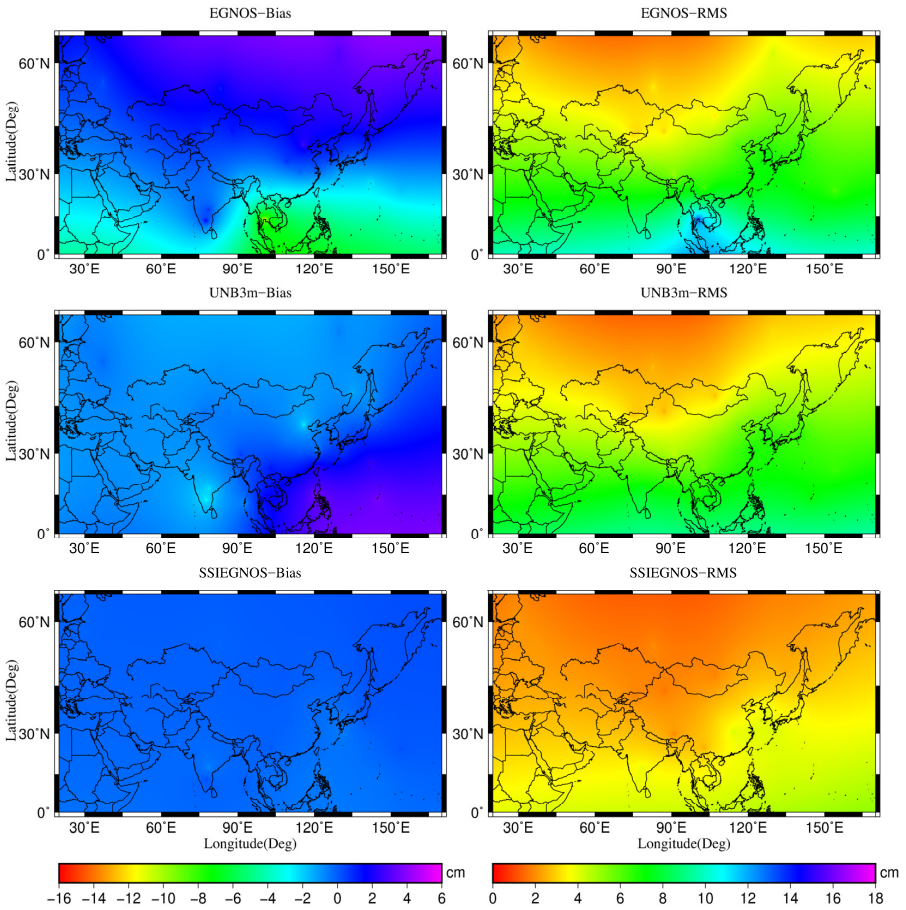

Figure 9. The distribution of the annual predicted bias and RMS error of the EGNOS, UNB3m, and SSIEGNOS models over Asia in 2011. The color denotes the magnitudes of the annual predicted bias and RMS error.

Table 2. Statistics of predicted bias and RMS error of the EGNOS, UNB3m, and SSIEGNOS models over Asia.

	EGNOS	**UNB3m**	**SSIEGNOS**
Bias (cm)	−0.2 [−17.5, 4.0]	0.2 [−4.0, 5.6]	−0.1 [−1.4, 0.8]
RMS (cm)	6.1 [1.9, 18.6]	5.4 [1.7, 8.6]	3.1 [1.3, 4.8]

Note: Values in brackets show the minima and maxima of the bias and RMS error for all 46 IGS sites in 2011.

Figure 10 shows histograms of the annual bias and RMS error of the EGNOS, UNB3m, and SSIEGNOS models. The variation of the annual bias in the SSIEGNOS model is between −1.4 cm and 0.8 cm and the RMS error is between 1.3 cm and 4.8 cm. In Figure 10, the histograms of both bias and RMS error of the SSIEGNOS model are much more centralized than those of the EGNOS

and UNB3m models. Figures 9 and 10 and Table 2 show apparently that the SSIEGNOS model yields higher predicted precision than the EGNOS and UNB3m models in Asia, with results comparable with the ZTD calculation using the ECMWF reanalysis data [12].

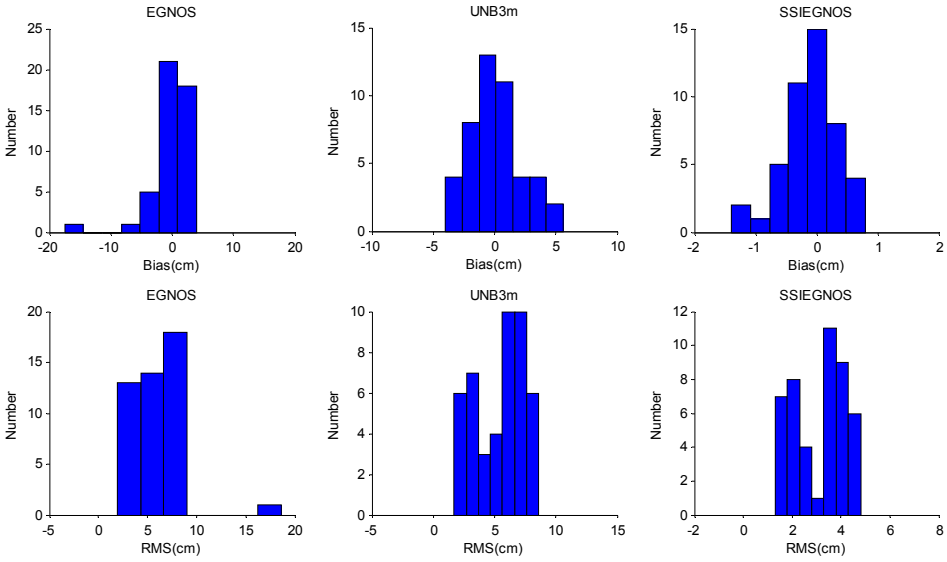

Figure 10. Distribution histogram of predicted bias and RMS error of the EGNOS, UNB3m, and SSIEGNOS models over Asia in 2011. The left shows the EGNOS model results, the middle shows the UNB3m model results, and the right shows the SSIEGNOS model results. The vertical axis denotes the number of samples.

To investigate the monthly and seasonal variations of predicted bias and RMS error in the SSIEGNOS model, one year of bias and RMS error from 46 sites in 2011 were used for monthly and seasonal statistics; the results are also compared with EGNOS and UNB3m models. The statistical results are shown in Figure 11.

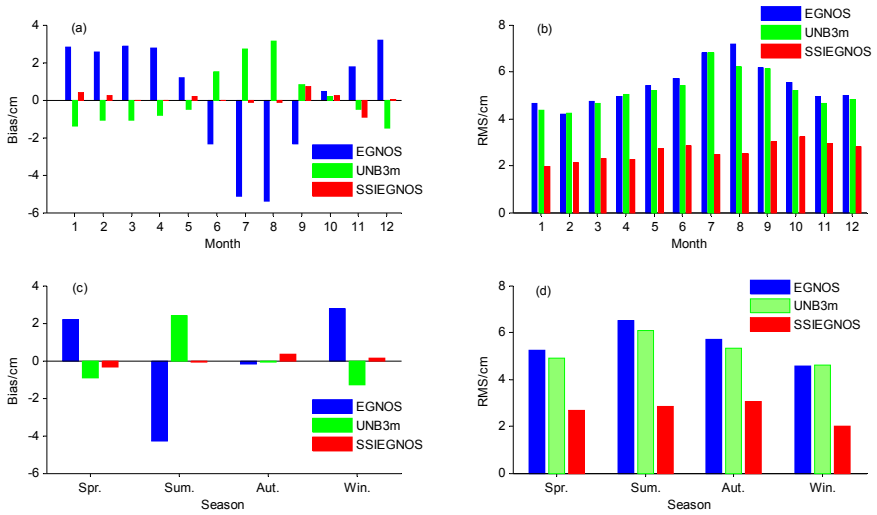

Figure 11. (**a**,**b**) and (**c**,**d**) show the monthly and seasonal variations of predicted bias and RMS error in 2011 over Asia using the EGNOS, UNB3m, and SSIEGNOS models, respectively. The blue color denotes the EGNOS model, the green color denotes the UNB3m model, and the red color denotes the SSIEGNOS model.

Figure 11 shows the monthly and seasonal variations of predicted bias without obvious regulation in the three models. The predicted RMS error shows apparent seasonal variations in both the EGNOS model and the UNB3m model, with larger values in summer and smaller values in winter. In the SSIEGNOS model, however, the predicted RMS error shows slight monthly variations, with lower values in winter and slightly larger values in autumn. Hence, the SSIEGNOS model has relatively small seasonal variations.

3.3.2. Investigation of the Long-Term Time Series of Predicted ZTD

As analyzed above, the annual variations of predicted RMS error in the SSIEGNOS model present obvious regional characteristics over Asia. Thus, we chose the IRKT (Northern Asian), PIMO (Southern Asian), POL2 (Western Asian), and TSK2 (Eastern Asian) sites as four typical IGS sites to investigate the feasibility of using the SSIEGNOS model to predict the long-term time series of ZTD. In this section, we utilize the SSIEGNOS model to predict two years of ZTD from 2011 to 2012 for the four typical IGS sites; the predicted results are also compared with the EGNOS and UNB3m models. Similarly, the two years of ZTD derived from the IGS center are regarded as reference values. Lastly, the variations of daily, monthly, seasonal, and annual predicted bias and RMS error are analyzed for the four sites, respectively.

First, we analyze the daily predicted bias and RMS error at the four sites from 2011 to 2012. In addition, two years of daily predicted bias and RMS error are analyzed using the normal distribution method; the statistical results are shown in Figures 12–15.

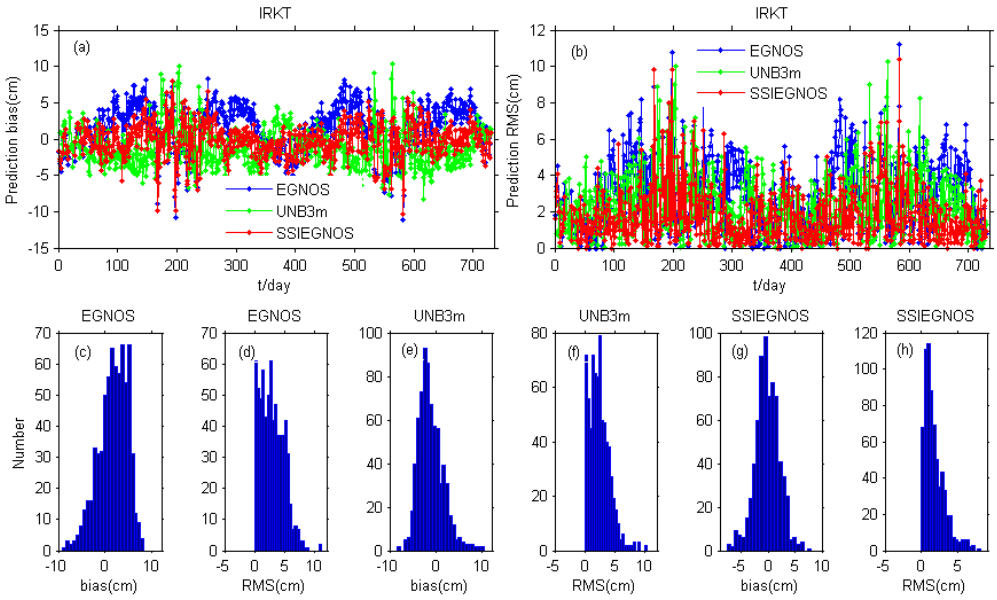

Figure 12. (**a**,**b**) Time series of daily predicted bias and RMS from 2011–2012 at the IRKT site. The blue line denotes the EGNOS model, the green line denotes the UNB3m model, and the red line denotes the SSIEGNOS model. (**c**–**h**) Histograms of the daily predicted bias and RMS error from 2011–2012 for the three models, respectively.

Figures 12–15 show that the daily predicted bias and RMS error in the SSIEGNOS model present significant stable and similar variations each year among the four IGS sites. Moreover, the SSIEGNOS model has remarkable refining results at the PIMO (Southern Asian) and TSK2 (Eastern Asian) sites, compared with the EGNOS and UNB3m models. We also find that the EGNOS model has a larger mean negative bias at the PIMO site and a positive mean bias at the IRKT and TSK2 sites; however, the UNB3m model shows reverse results at the PIMO, IRKT, and TSK2 sites. In the SSIEGNOS model, however, two years of daily predicted bias at the four sites are approximately yielded to the normal

distribution. Therefore, the SSIEGNOS model exhibits a more accurate performance relative to the EGNOS and UNB3m models, in terms of predicting the long-term time series of ZTD. We can easily determine that the ZTD prediction of the SSIEGNOS model displays similar behavior in 2011–2012. In other words, the SSIEGNOS model shows high stability when used to predict the long-term ZTD time series.

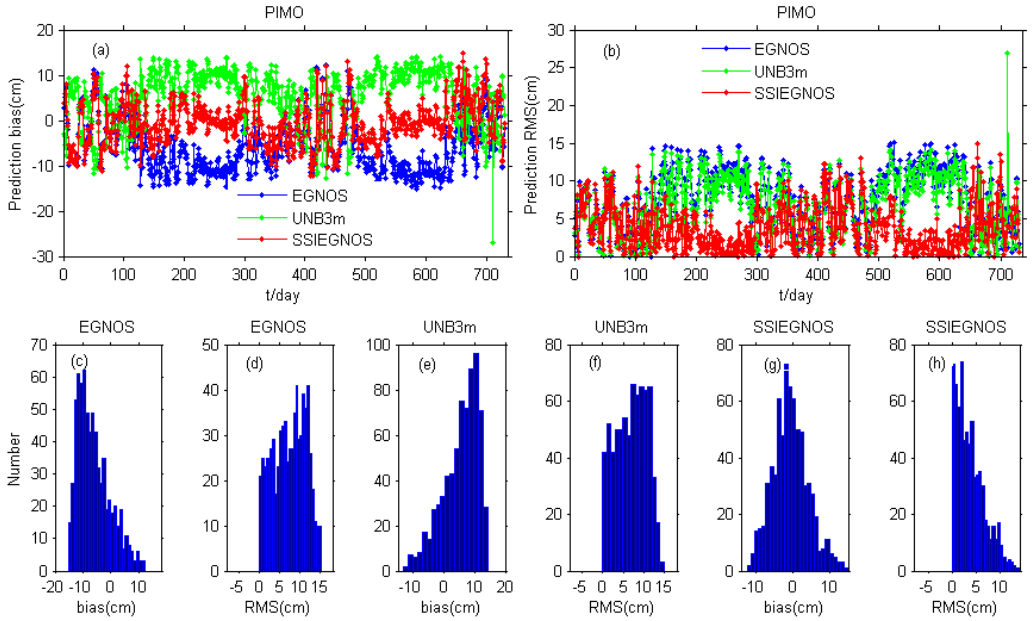

Figure 13. (**a**,**b**) Time series of daily predicted bias and RMS error from 2011–2012 at the PIMO site. The blue line denotes the EGNOS model, the green line denotes the UNB3m model, and the red line denotes the SSIEGNOS model. (**c**–**h**) Histograms of the daily predicted bias and RMS error from 2011–2012 for the three models.

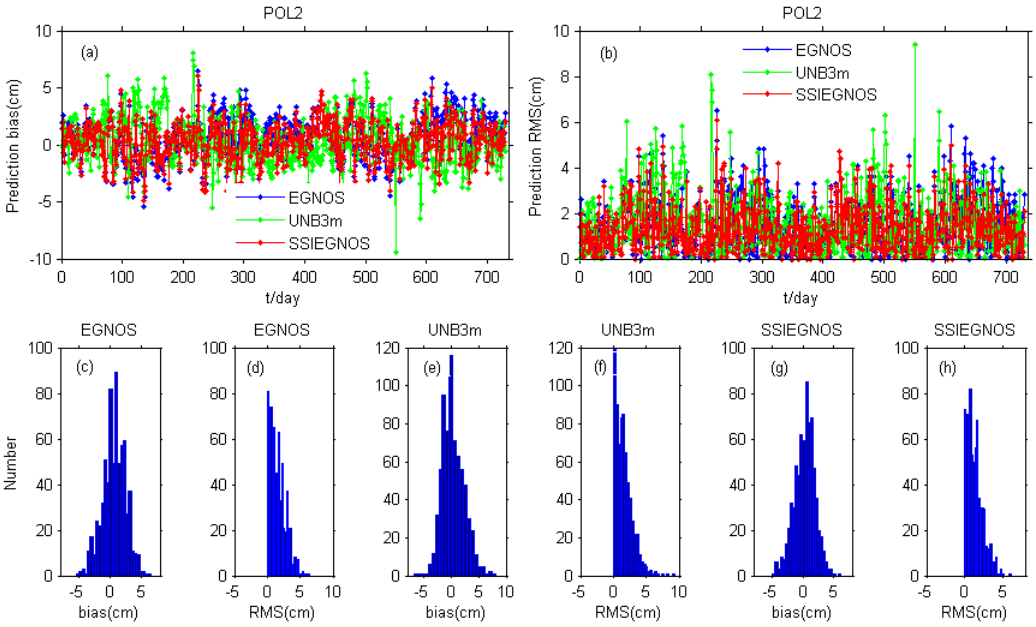

Figure 14. (**a**,**b**) Time series of daily predicted bias and RMS error from 2011–2012 at the POL2 site. The blue line denotes the EGNOS model, the green line denotes the UNB3m model, and the red line denotes the SSIEGNOS model. (**c**–**h**) Histograms of the daily predicted bias and RMS error from 2011–2012 for the three models.

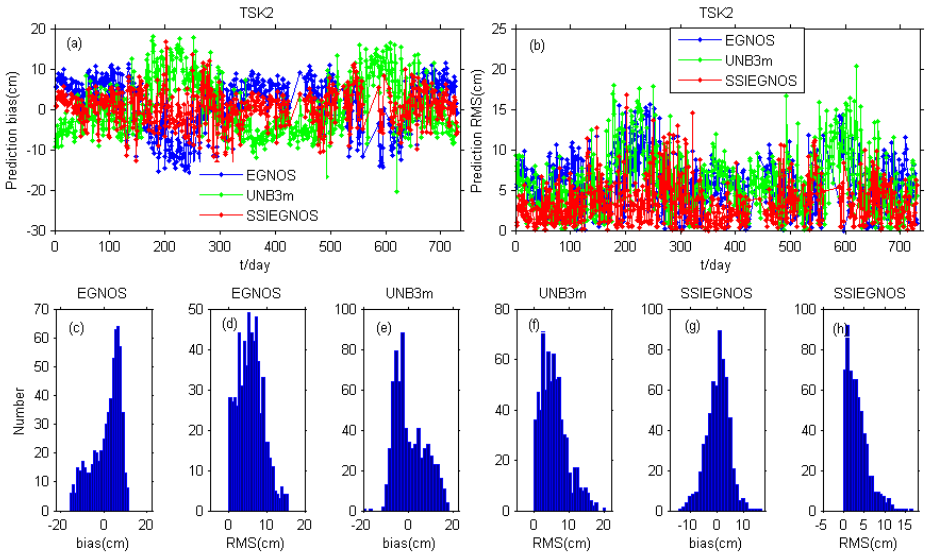

Figure 15. (**a**,**b**) Time series of daily predicted bias and RMS error from 2011–2012 at the TSK2 site. The blue line denotes the EGNOS model, the green line denotes the UNB3m model, and the red line denotes the SSIEGNOS model. (**c**–**h**) Histograms of the daily predicted bias and RMS error from 2011–2012 for the three models.

Figure 14 shows that the SSIEGNOS model has a slightly poorer refining performance at the POL2 site, compared with the EGNOS and UNB3m models. The POL2 site is located in the high-latitude area of Asia, thus both the EGNOS model and the UNB3m model exhibit a strong performance in calculating the ZTD in this region. Hence, a slightly poorer refining result is obtained in this region using the SSIEGNOS model. Even so, the SSIEGNOS model can still maintain an adequate performance in predicting the long-term ZTD time series in the high-latitude area of Asia.

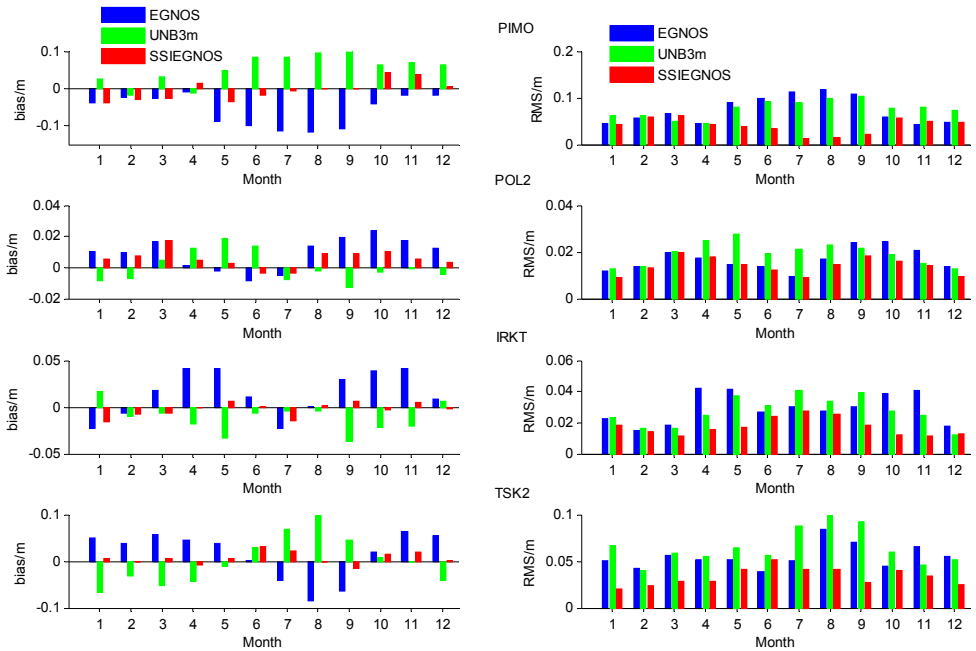

Figure 16. Monthly mean predicted bias and RMS from 2011–2012 at the TSK2, POL2, IRKT, and TSK2 sites. The blue bars, green bars, and red bars denote the monthly bias and RMS error of the EGNOS, UNB3m, and SSIEGNOS models, respectively.

Furthermore, the monthly and seasonal mean predicted bias and RMS error are analyzed for the three models. The results are shown in Figures 16 and 17.

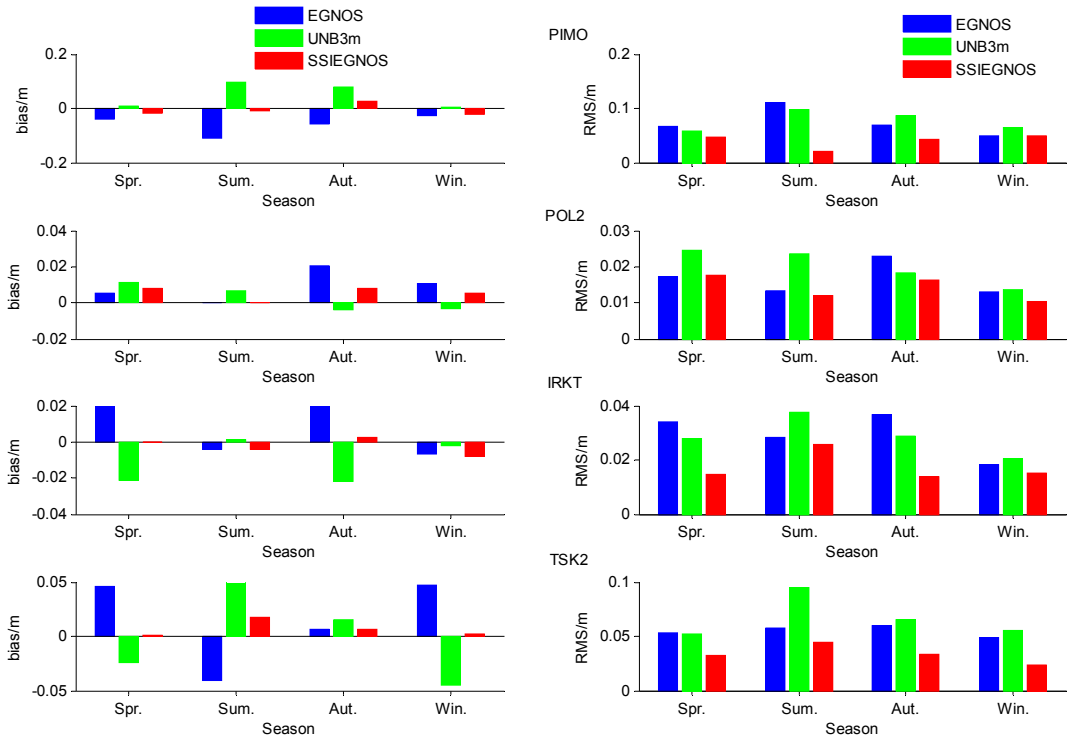

Figure 17. Seasonal mean predicted bias and RMS error from 2011–2012 at the TSK2, POL2, IRKT, and TSK2 sites. The blue bars, green bars and red bars denote the monthly bias and RMS error of the EGNOS, UNB3m, and SSIEGNOS models, respectively.

Figures 16 and 17 show that the SSIEGNOS model shows no consistent variations in the monthly and seasonal mean predicted bias and RMS error, especially in terms of the RMS error, which presents low values in summer at the PIMO and POL2 sites. On the contrary, the other two sites show larger values in summer. The SSIEGNOS model also exhibits higher accuracy in terms of monthly and seasonal mean predicted bias and RMS error than the EGNOS and UNB3m models in each month from 2011 to 2012.

Lastly, Table 3 indicates that the annual predicted bias and RMS error of the SSIEGNOS model between 2011 and 2012 present small changes at the four sites. Hence, the SSIEGNOS model exhibits significant stability when used to predict the long-term time series of ZTD.

Table 3. Annual predicted bias and RMS error from 2011–2012 at the TSK2, POL2, IRKT, and TSK2 sites for the EGNOS, UNB3m, and SSIEGNOS models (Unit: cm).

Site Name	EGNOS				UNB3m				SSIEGNOS			
	2011		2012		2011		2012		2011		2012	
	Bias	**RMS**	**Bias**	**RMS**	**Bias**	**RMS**	**Bias**	**RMS**	**Bias**	**RMS**	**Bias**	**RMS**
PIMO	−6.24	8.36	−5.90	7.45	3.94	8.00	5.57	7.80	−0.84	3.57	−0.48	4.03
TSK2	0.78	6.96	2.04	5.37	1.10	6.93	0.17	5.90	0.08	3.53	0.65	3.29
POL2	0.45	1.89	0.89	1.66	0.57	2.17	0.01	1.75	0.10	1.36	0.56	1.40
IRKT	1.71	3.54	1.52	2.94	1.09	3.02	1.13	2.89	−0.11	1.88	−0.23	1.73

In conclusion, the SSIEGNOS model displays remarkable stability and higher accuracy when used to predict the long-term ZTD time series, which, without any meteorological data, can only

relate to the time and position of site. In the future, the parameters of the SSIEGNOS model for each station can be updated using the latest three years of IGS ZTD derived from IGS center. Thus, we can utilize the updated parameters of SSIEGNOS to predict the next one or two years of ZTD for each station. Therefore, we suggest that the SSIEGNOS model can be employed as a real-time single site tropospheric correction model for VLBI technique or other space geodetic techniques in Asia.

4. Conclusions

In this study, five years of ZTD data from 2008 to 2012 of 46 IGS sites distributed in Asia were used to investigate the performance of the SSIEGNOS model. The results are as follows:

(1) Relative to the IGS-observed ZTD, the bias and RMS error of the ZTD calculated from the EGNOS model are 0.12 cm and 5.87 cm, respectively, whereas those of the SSIEGNOS model are 0.00 cm and 2.52 cm, respectively. Moreover, the SSIEGNOS model exhibits higher predicted precision at latitudes lower than 30 degrees.

(2) The EGNOS model shows seasonal variations in terms of the bias and RMS error. The SSIEGNOS model shows slight variations and has a better refining performance in summer compared with the EGNOS model. The relation between the bias with altitude, longitude, and latitude are not obvious for the two models, but the RMS error generally decreases with increasing altitude and latitude. In addition, the SSIEGNOS model has a significant correction effect in low-latitude areas.

(3) The SSIEGNOS model shows remarkable stability and higher accuracy than both the EGNOS model and the UNB3m model when used to predict the long-term ZTD time series, even without any meteorological data, whereas the EGNOS and UNB3m models show comparable predicted results. Therefore, we can regard the SSIEGNOS model as the real-time single site tropospheric correction model of GNSS, VLBI, and DORIS in Asia.

(4) The SSIEGNOS model is in the same form in Asia, only the parameters are different in different sites, so the SSIEGNOS model can be used for those sites located in Asia if equipped with permanent GNSS receivers. In future works, multi-source data fusion for refining the EGNOS model over Asia or global area should be examined, as it is likely to further improve accuracy.

Acknowledgments: This work was sponsored by the National Natural Foundation of China (41541032 and 41664002); the "Ba Gui Scholars" program of the provincial government of Guangxi, Guangxi Natural Science Foundation of China (2015GXNSFAA139230 and 2012GXNSFGA060001); the Guangxi Key Laboratory of Spatial Information and Geomatics (14-045-24-10); and the basic ability promotion program for young and middle-aged teachers of Guangxi (KY2016YB189). We thank the international IGS center for providing tropospheric products.

Author Contributions: Liangke Huang conceived and designed the experiments, Liangke Huang performed the modeling, Shaofeng Xie and Lilong Liu analyzed the data, Lilong Liu and Chuanli Kang gave relevant technical support, all authors discussed the basic structure of the manuscript, Liangke Huang finished the first draft, and Shaofeng Xie, Junyu Li, and Jun Chen reviewed and edited the draft. All authors read and approved the manuscript.

Conflicts of Interest: The authors declare no conflict of interest.

References

1. Li, W.; Yuan, Y.B.; Ou, J.K.; Li, H.; Li, Z.S. A global zenith tropospheric delay model IGGtrop for GNSS applications. *Chin. Sci. Bull.* **2012**, *57*, 1317–1325. [CrossRef]
2. Shi, J.B.; Gao, Y. A troposphere constraint method to improve PPP ambiguity-resolved height solution. *J. Navig.* **2014**, *67*, 249–262. [CrossRef]
3. Yao, Y.B.; Yu, C.; Hu, Y.F. A new method to accelerate PPP convergence time by using a global zenith troposphere delay estimate model. *J. Navig.* **2014**, *67*, 899–910. [CrossRef]
4. Flores, A.; Ruffini, G.; Rius, A. 4D tropospheric tomography using GPS slant wet delays. *Ann. Geophys.* **2000**, *18*, 223–234. [CrossRef]
5. Haase, J.; Ge, M.R.; Vedel, H.; Calais, E. Accuracy and variability of GPS tropospheric delay measurements of water vapor in the Western Mediterranean. *J. Appl. Meteor.* **2003**, *42*, 1547–1568. [CrossRef]

6. Basili, P.; Bonafoni, S.; Ferrara, R. Assessment of precipitable water vapour by use of a local GPS network and microwave ground-based radiometer. *IEEE Antennas Wirel. Propag. Lett.* **2003**, *2*, 72–76.
7. Bonafoni, S.; Mazzoni, A.; Cimini, D.; Montopoli, M.; Pierdicca, N.; Basili, P.; Ciotti, P.; Carlesimo, G. Assessment of water vapor retrievals from a GPS receiver network. *GPS Solut.* **2013**, *17*, 475–484. [CrossRef]
8. Farah, A.; Moore, T.; Hill, C.J. High spatial variation tropospheric model for GPS-data simulation. *J. Navig.* **2005**, *58*, 459–470. [CrossRef]
9. Bromwich, D.H.; Wang, S.H. Evaluation of the NCEP-NCAR and ECMWF 15-and 40-yr reanalyses using Rawinsonde data from two independent Arctic field experiments. *Mon. Weather Rev.-Spec. Sect.* **2005**, *133*, 3562–3578. [CrossRef]
10. Boehm, J.; Werl, B.; Schuh, H. Troposphere mapping functions for GPS and very long baseline interferometry from European Centre for Medium-Range Weather Forecasts operational analysis data. *J. Geophys. Res.* **2006**, *111*, B02406. [CrossRef]
11. Ibrahim, H.E.; EI-RRabbany, A. Regional stochastic models for NOAA-based residual tropospheric delays. *J. Navig.* **2008**, *61*, 209–219. [CrossRef]
12. Chen, Q.M.; Song, S.L.; Heise, S.; Liou, Y.; Zhu, W.Y.; Zhao, J.Y. Assessment of ZTD derived from ECMWF/NCEP data with GPS ZTD over China. *GPS Solut.* **2011**, *15*, 415–425. [CrossRef]
13. Chen, Q.M.; Song, S.L.; Zhu, W.Y. An analysis of the accuracy of zenith tropospheric delay calculated from ECMWF/NCEP data over Asian area. *Chin. J. Geophys.* **2012**, *55*, 1541–1548. [CrossRef]
14. Collins, J.P.; Langley, R.B. *A Tropospheric Delay Model for the User of the Wide Area Augmentation System*; Department of Geodesy and Geomatics Engineering, University of New Brunswick: Fredericton, NB, Canada, 1997.
15. Krueger, E.; Schuler, T.; Hein, G.W.; Martellucci, A.; Blarzino, G. Galileo tropospheric correction approaches developed within GSTB-V1. In Proceedings of the ENC-GNSS 2004, Rotterdam, The Netherlands, 16–19 May 2004.
16. Schuler, T. The TropGrid2 standard tropospheric correction model. *GPS Solut.* **2014**, *18*, 123–131. [CrossRef]
17. Lagler, K.; Schindelegger, M.; Boehm, J.; Krásná, H.; Nilsson, T. GPT2: Empirical slant delay model for radio space geodetic techniques. *Geophys. Res. Lett.* **2013**, *40*, 1069–1073. [CrossRef] [PubMed]
18. Böhm, J.; Heinkelmann, R.; Schuh, H. Short Note: A global model of pressure and temperature for geodetic applications. *J. Geod.* **2007**, *81*, 679–683. [CrossRef]
19. Böhm, J.; Moeller, G.; Schindelegger, M.; Pain, G.; Weber, R. Development of an improved empirical model for slant delays in the troposphere (GPT2w). *GPS Solut.* **2015**, *19*, 433–441. [CrossRef]
20. Yao, Y.B.; Xu, C.Q.; Shi, J.B.; Cao, N.; Zhang, B.; Yang, J.J. ITG: A new global GNSS tropospheric correction model. *Sci. Rep.* **2015**. [CrossRef] [PubMed]
21. Yao, Y.B.; Zhang, B.; Xu, C.Q.; He, C.Y.; Yu, C.; Yan, F. A global empirical model for estimating zenith tropospheric delay. *Sci. China Earth Sci.* **2016**, *59*, 118–128. [CrossRef]
22. Tomislav, K.; Maja, B.; Ivan, M. Evaluation of EGNOS tropospheric delay model in south-eastern Europe. *J. Navig.* **2009**, *62*, 341–349.
23. Penna, N.; Dodson, A.; Chen, W. Assessment of EGNOS tropospheric correction model. *J. Navig.* **2001**, *54*, 37–55. [CrossRef]
24. Bock, O.; Willis, P.; Lacarra, M.; Bosser, P. An inter-comparison of zenith tropospheric delays derived from DORIS and GPS data. *Adv. Space Res.* **2010**, *46*, 1648–1660. [CrossRef]
25. Teke, K.; Böhm, J.; Nilsson, T.; Schuh, H.; Steigenberger, P.; Dach, R.; Heinkelmann, R.; Willis, P.; Haas, R.; Garcia-Espada, S.; et al. Multi-technique comparison of troposphere zenith delays and gradients during CONT08. *J. Geod.* **2011**, *85*, 395–413. [CrossRef]
26. Wei, H.H.; Jin, S.G.; He, X.F. Effects and disturbances on GPS-derived zenith tropospheric delay during the CONT08 campaign. *Adv. Space Res.* **2012**, *50*, 632–641. [CrossRef]
27. Ning, T.; Haas, R.; Elgered, G.; Willen, U. Multi-technique comparisons of 10 years of wet delay estimations on the West Coast of Sweden. *J. Geod.* **2012**, *86*, 565–575. [CrossRef]
28. Teke, K.; Nilsson, T.; Böhm, J.; Hobiger, T.; Steigenberger, P.; Garcia-Espada, S.; Haas, R.; Willis, P. Tropospheric delays from space geodetic techniques, water vapor radiometers, and numerical weather models over a series of continuous VLBI campaigns. *J. Geod.* **2013**, *87*, 981–1001. [CrossRef]
29. Huang, Y.; Chang, S.Q.; Li, P.J.; Hu, X.G.; Wang, G.L.; Liu, Q.H.; Zheng, W.M.; Fan, M. Orbit determination of Chang'E-3 and positioning of the lander and the rover. *Chin. Sci. Bull.* **2014**, *59*, 3858–3867. [CrossRef]

30. Lou, Y.D.; Liu, Y.; Shi, C.; Wang, B.; Yao, X.G.; Zheng, F. Precise orbit determination of BeiDou constellation: Method comparison. *GPS Solut.* **2016**, *20*, 259–268. [CrossRef]
31. Ping, J.S.; Su, X.L.; Huang, Q.; Yan, J.G. The Chang'E-1 orbiter plays a distinctive role in China's first successful selenodetic lunar mission. *Sci. Chin. Phys. Mech. Astron.* **2011**, *54*, 2130–2144. [CrossRef]
32. Hefty, J.; Gontier, A. Sensitivity of UT1 determined by single-baseline VLBI to atmospheric delay model, terrestrial and celestial reference frames. *J. Geod.* **1997**, *71*, 253–261. [CrossRef]
33. Hobiger, T.; Otsubo, T. Combination of GPS and VLBI on the observation level during CONT11—Common parameters, ties and inter-technique biases. *J. Geod.* **2014**, *88*, 1017–1028. [CrossRef]
34. Nilsson, T.; Karbon, M.; Soja, B.; Heinkelmann, R.; Lu, C.X.; Schuh, H. Atmospheric modeling for co-located VLBI antennas and twin telescopes. *J. Geod.* **2015**, *89*, 655–665. [CrossRef]
35. Böhm, J.; Schuh, H.; Weber, R. Influence of tropospheric zenith delays obtained by GPS and VLBI on station heights. *Vert. Ref. Syst.* **2002**, *124*, 107–112.
36. Deblonde, G.; Macpherson, S.; Mireault, Y.; Heroux, P. Evaluation of GPS precipitable water over Canada and the IGS network. *J. Appl. Meteor.* **2005**, *44*, 153–166. [CrossRef]
37. Byun, S.H.; Bar-Sever, Y.E. A new type of troposphere zenith path delay product of the international GNSS service. *J. Geod.* **2009**, *83*, 367–373. [CrossRef]
38. Leandro, R.F.; Langley, R.B.; Santos, M.C. UNB3m_pack: A neutral atmosphere delay package for radiometric space techniques. *GPS Solut.* **2008**, *12*, 65–70. [CrossRef]